Towards deterministically controlled InGaAs/GaAs lateral quantum dot molecules

To cite this article: L Wang *et al* 2008 *New J. Phys.* **10** 045010

View the article online for updates and enhancements.

Related content

Recent citations

Towards deterministically controlled InGaAs/GaAs lateral quantum dot molecules

L Wang[1,4]**, A Rastelli**[1,2]**, S Kiravittaya**[1]**, P Atkinson**[1]**, F Ding**[2]**,
C C Bof Bufon**[2]**, C Hermannstädter**[3]**, M Witzany**[3]**,
G J Beirne**[3]**, P Michler**[3] **and O G Schmidt**[1,2]

[1] Max-Planck-Institut für Festkörperforschung, Heisenbergstrasse 1,
D-70569 Stuttgart, Germany
[2] Institute for Integrative Nanosciences, IFW Dresden,
Helmholtzstrasse 20, D-01069 Dresden, Germany
[3] Institut für Halbleiteroptik und Funktionelle Grenzflächen,
Universität Stuttgart, Allmandring 3, D-70569 Stuttgart, Germany
E-mail: l.wang@fkf.mpg.de

Abstract. We report on the fabrication, detailed characterization and modeling of lateral InGaAs quantum dot molecules (QDMs) embedded in a GaAs matrix and we discuss strategies to fully control their spatial configuration and electronic properties. The three-dimensional morphology of encapsulated QDMs was revealed by selective wet chemical etching of the GaAs top capping layer and subsequent imaging by atomic force microscopy (AFM). The AFM investigation showed that different overgrowth procedures have a profound consequence on the QDM height and shape. QDMs partially capped and annealed *in situ* for micro-photoluminescence spectroscopy consist of shallow but well-defined quantum dots (QDs) in contrast to misleading results usually provided by surface morphology measurements when they are buried by a thin GaAs layer. This uncapping approach is crucial for determining the QDM structural parameters, which are required for modeling the system. A single-band effective-mass approximation is employed to calculate the confined electron and heavy-hole energy levels, taking the geometry and structural information extracted from the uncapping experiments as inputs. The calculated transition

---

[4] Author to whom any correspondence should be addressed.

IOP Institute of Physics Φ DEUTSCHE PHYSIKALISCHE GESELLSCHAFT

energy of the single QDM shows good agreement with the experimentally observed values. By decreasing the edge-to-edge distance between the two QDs within a QDM, a splitting of the electron (hole) wavefunction into symmetric and antisymmetric states is observed, indicating the presence of lateral coupling. Site control of such lateral QDMs obtained by growth on a pre-patterned substrate, combined with a technology to fabricate gate structures at well-defined positions with respect to the QDMs, could lead to deterministically controlled devices based on QDMs.

Contents

1. Introduction

Coupled semiconductor quantum dots (QDs) are attracting growing interest due to their potential application as solid-state quantum gates [1, 2]. Substantial progress towards the experimental implementation of such QD molecules (QDMs) has been achieved in the last few years both for electrically defined QDs (see [3] and references therein) and for self-assembled, vertically stacked QDs [4]–[7]. In the latter case, the distance between QDs in a QDM is well defined and the signature of coupling consists in anticrossing patterns [8] in the photoluminescence (PL) spectra versus the applied vertical electric field, necessary to bring the QDs into resonance. To explore the possibility of coupling a larger number of self-assembled QDs, investigations on lateral coupling are needed [9, 10]. While vertical QDMs have been extensively studied, much less work has been carried out on the lateral geometry, because special growth protocols are required [11]–[16] and it is difficult to fabricate controlled structures in the planar geometry. Recently, we have reported a method to fabricate lateral QDMs [9, 11], [17]–[20] and direct observation of coupling has been presented based on electric field-dependent PL spectroscopy and photon statistics experiments [19, 20, 21].

In contrast to vertically stacked QDs, in lateral QDMs not only the size of the QDs, but also the interdot spacing, is affected by inherent fluctuations, and coupling depends strongly on these parameters. Moreover, a satisfactory determination and a comprehensive understanding of the morphology of encapsulated QDMs are still missing. For this reason, it is important to study in detail the structural properties of embedded QDMs. Here, we use selective etching to obtain the three-dimensional (3D) shape/size and the spacing between InGaAs QDs composing the QDMs. Based on this obtained structural information, we estimate the coupling energy using

a single-band effective-mass approximation. As the interdot distance decreases, the electron (hole) wavefunction splits into symmetric (bonding) and antisymmetric (antibonding) states, indicating that the two QDs are quantum mechanically coupled and the carrier probability distribution is spreading over the two dots. This behavior is consistent with the recent more detailed calculation of exciton spectra in lateral QDMs in an electric field [22, 23]. The coupling energy increases when the interdot distance decreases. The InGaAs QDMs show good optical properties and a strong experimental indication of coupling has been reported [19].

In order to obtain deterministically controlled structures, we propose: (i) fabrication of QDMs on a pre-patterned substrate to achieve control on QDM position, and (ii) possible triple-terminal devices, which would allow not only bringing two QDs into resonance by two side gates, but also tuning of the coupling strength by applying a potential to the middle gate [11]. Integrating such gate structures at well-defined positions with respect to ordered QDMs could lead to deterministically controlled devices based on QDMs.

2. Fabrication of lateral InGaAs QDMs

Molecular beam epitaxy combined with $AsBr_3$ *in situ* selective etching of buried InAs QDs is used to fabricate InGaAs QDMs. The growth process starts with a layer of high-density InAs QDs, capped by 60 nm GaAs at 500 °C. This layer sequence allows us to obtain a surface with stepped mounds that will guide the formation of QDs and improve the yield of QDMs [18]. In order to create QDMs, a second InAs QD layer is deposited subsequently on this surface and overgrown by 10 nm GaAs followed by an $AsBr_3$ *in situ* etching step. Taking advantage of preferential etching for InGaAs over GaAs and a strain-enhanced etching rate, buried QDs will be removed and nanoholes formed at the positions previously occupied by QDs [11, 17]. Overgrowth of the nanoholes with InAs of more than 1.8 monolayers (MLs) results in the formation of QDMs aligned in the [1$\bar{1}$0] crystal direction. The samples are cooled down immediately to room temperature and the surface morphology of the samples is characterized by atomic force microscopy (AFM) in tapping mode. For the PL investigations, the QDMs are partially capped with 2 nm GaAs at 500 °C and annealed *in situ* for 4 min to blueshift the emission and then embedded in a GaAs matrix [24].

Figure 1 shows snapshots of the surface morphology and schematics during different stages of the QDM formation process. The InAs QDs, grown on stepped mounds, have an average height of about 12.8 nm and a surface density of 3×10^9 cm^{-2} (figure 1(a)). The mounds, composed of several MLs of GaAs, are elongated in the [1$\bar{1}$0] direction because of the anisotropic diffusion of GaAs. It is interesting to note that all the QDs are nucleated at the convex edges of the mounds [25, 26], which is ascribed to the maximal strain relaxation at these sites [25]. After an overgrowth step by 10 nm GaAs, we utilize $AsBr_3$ selective etching to create bow-tie-shaped nanoholes slightly elongated in the [110] direction, as shown in figure 1(b). Besides the nanoholes, the mound structures can still be recognized even if the selective etching produces some surface roughness.

Once the nanoholes are overgrown with 1 ML of InAs, the surface becomes atomically flat and stepped mounds with well-defined atomic steps are clearly visible (see figure 1(c)). Neither a trace of the nanoholes nor the precursors for the QDMs are observed at this stage since the nanoholes are filled up with InGaAs [11] prior to the QDM formation. The filling up of the nanoholes can be explained by the concave surface curvature together with In–Ga intermixing at this growth temperature [18]. The joined effect of these two processes results in the formation
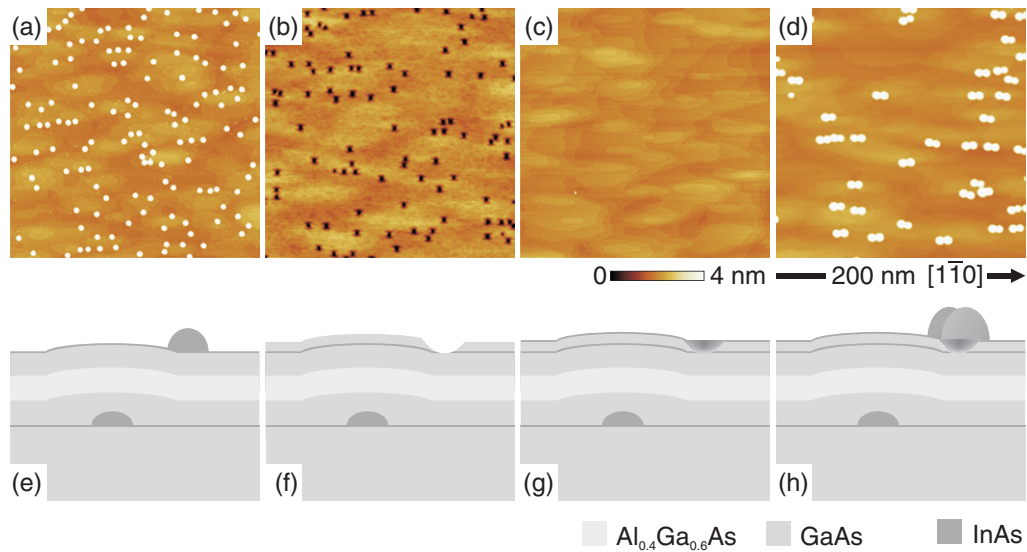
Figure 1. AFM images of (a) InAs QDs grown on a surface composed of stepped mounds formed by buried InAs QDs, (b) nanoholes, (c) nanoholes overgrown with 1 ML of InAs and (d) InAs QDMs. Figures (e)–(h) represent corresponding schematics of the sample structures in the [110] direction.

of a flat surface with an inhomogeneous In profile inside the holes, higher at the center of the filled nanoholes. When more InAs is supplied, QDs form at the regions around the center of the filled holes due to lowering of the strain energy [18]. In addition, the influence of the strain relaxation at the step edges will guide these QDs to form preferentially into QDMs aligned along the [1$\bar{1}$0] direction at the convex sides of the stepped mounds, shown in figure 1(d).

Micro-PL represents the easiest way to access and investigate the coupling behavior of single QDMs. For this purpose, a low surface density is required to ensure that only one QDM is being measured. Figure 2(a) shows a representative AFM image of low-density ($4 \times 10^7 \, \text{cm}^{-2}$) uncapped QDMs grown on stepped mounds. For the PL measurement, they are first treated by partial capping and annealing (PCA) to blueshift the emission [24] and then further embedded in a GaAs matrix, which makes them inaccessible to AFM characterization. It is well known that both the size and shape of QDs change dramatically during the capping process [27, 28]. As a consequence, the structural information obtained for as-grown QDMs cannot be applied directly to QDMs once they are encapsulated.

In this case, cross-sectional transmission electron microscopy (TEM) might be helpful to determine the QDM structural properties. However, as illustrated in figure 2(b), the low density renders the probability of catching a QDM in cross-section so small that only single QDs in the buried high-density QD layer can be detected. Moreover, the full 3D structure of the buried QDMs cannot be deduced from cross-sectional analysis.

3. Revealing the morphology of QDMs by selective etching

In order to obtain insights into the QDM morphology, two different approaches based on selective etching and AFM characterization are employed. The first approach consists in using
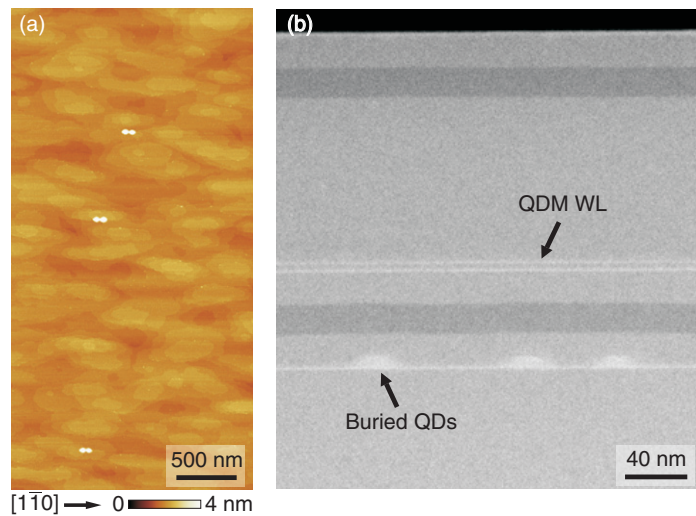
Figure 2. (a) AFM image of low density InAs QDMs and (b) a cross-sectional TEM image of low density QDM sample for PL characterization adapted from [21]. Buried QDs and wetting layer (WL) of QDMs are indicated.

$AsBr_3$ to remove *in situ* the InGaAs material composing the InGaAs QDMs partially overgrown with GaAs. As discussed below, this technique provides qualitative information on the size of the QDs composing a QDM and on the interdot distance.

For this investigation, QDMs treated by 2 nm GaAs partial capping and 4 min annealing are of special interest since the same growth protocol is applied on the sample for PL measurements. After the PCA procedure, an $AsBr_3$ etching step with a nominal depth of 0.5 nm is applied. The nominal etching depth is defined as the etching depth for planar GaAs under the same condition. Figure 3(d) shows the surface morphology of the QDM sample treated with PCA and 0.5 nm $AsBr_3$ selective etching. Double holes with a slightly smaller diameter than the as-grown QDMs in figure 3(a) are obtained, showing that the buried QDMs are removed. The high etching selectivity for In-rich material and strain account for the formation of double holes. The *in situ* etching allows us to obtain qualitative information from the buried QDMs. However, a quantitative determination of the QDM structural parameters is limited by the choice of etching depth, since it is hard to verify whether the buried QDMs are completely removed or some residue from the QDMs still remains after 0.5 nm etching.

The second approach consists in an *ex situ* removal of the GaAs capping layer by means of ammonium hydroxide (28% NH_4OH), hydrogen peroxide (31% H_2O_2), and deionized water (1 : 1 : 25) combined with the characterization by AFM [29]. Figure 3(b) shows a representative AFM image of QDMs partially capped with 2 nm GaAs at 500 °C, *in situ* annealed for 4 min followed by 8 nm GaAs overgrowth. Shallow, elongated mounds are observed, as also reported in [27]. A close inspection shows that there are two height maxima at the center of each mound along the [1$\bar{1}$0] direction, indicating the position of the underlying QDM. To investigate the impact of different overgrowth procedures on the QDM morphology, another sample is grown and the QDMs are capped at an initial substrate temperature of 470 °C and 10 nm GaAs is deposited while the substrate temperature is ramped back to 500 °C. In this case, low-temperature capping results in two overlapped rhombic-shaped islands, each with a tiny hole in the middle (see figure 3(c)).
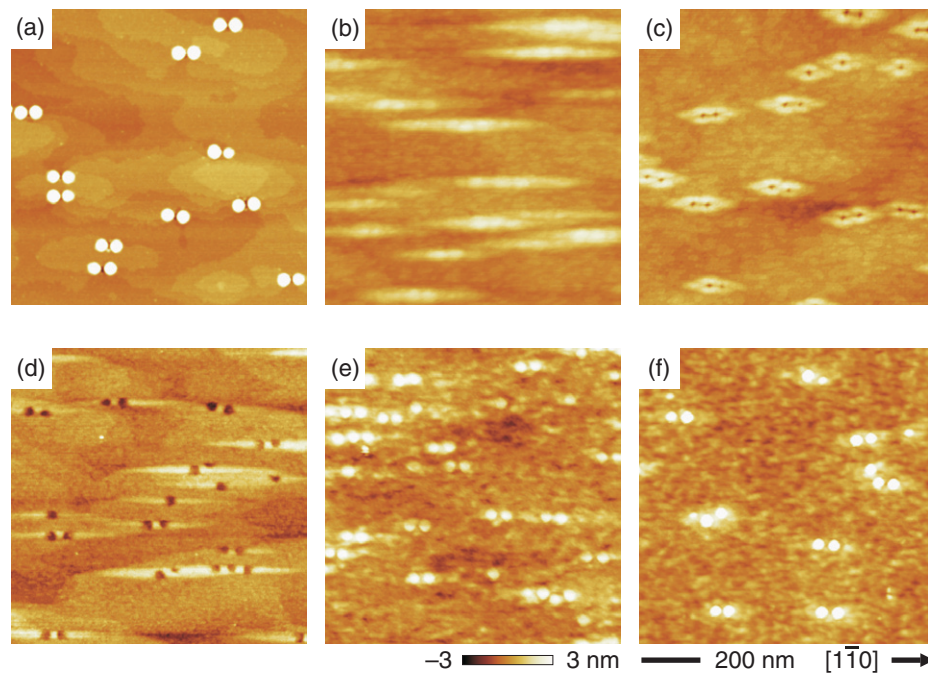
Figure 3. AFM images of (a) as-grown InAs QDMs, (b) QDMs capped by PCA, (c) QDMs capped at a low temperature, (d) double holes produced by AsBr$_3$ selective etching of buried QDMs, and (e) and (f) QDMs after the removal of the GaAs cap for samples corresponding to (b) and (c), respectively.

The remarkable differences in morphology for the two capping processes can be traced back to surface diffusion of GaAs at different growth conditions. In the former case, the first 2 nm GaAs is grown at a relatively high temperature, which enhances both the mobility of the Ga adatom on the surface and the In–Ga intermixing. During the annealing process, the mounds are further razed and the anisotropic surface diffusion becomes more pronounced, leading to the very anisotropically elongated mounds. For the latter case, the Ga diffusion is reduced at 470 °C and the unfavored growth of GaAs on top of InAs QDs results in tiny holes on top of each dot [27]–[31].

For the purpose of selective removal of the GaAs cap, the above two samples are then dipped into the etching solution and characterized by AFM. As shown in figures 3(e) and (f), we could distinguish the QDMs for each sample. In both cases, the heights of the QDMs are smaller than the as-grown sample. However, the average height of the QDMs after the PCA process is significantly smaller than that of low-temperature capped QDMs.

The statistical analysis of the size, height and interdot distance for the three samples revealed by etching is shown in figure 4. The as-grown QDMs have a broad distribution in height around 12 nm (see figure 4(a)). The overgrowth procedure at low substrate temperature causes a collapse of QDMs during the initial stage of overgrowth [27, 31], which results in a decrease of QDM height (see figure 4(b)). Capping at 500 °C followed by annealing leads to a more pronounced reduction of the QDM height to about 2.6 nm, shown in figure 4(c), mainly because of the migration of InAs away from the top of QDs [24, 28].

For the double holes produced by AsBr$_3$ *in situ* selective etching of QDMs (figure 4(d)), the average hole depth has a value of about 2.8 nm. Since a nominal 0.5 nm deep AsBr$_3$ etching
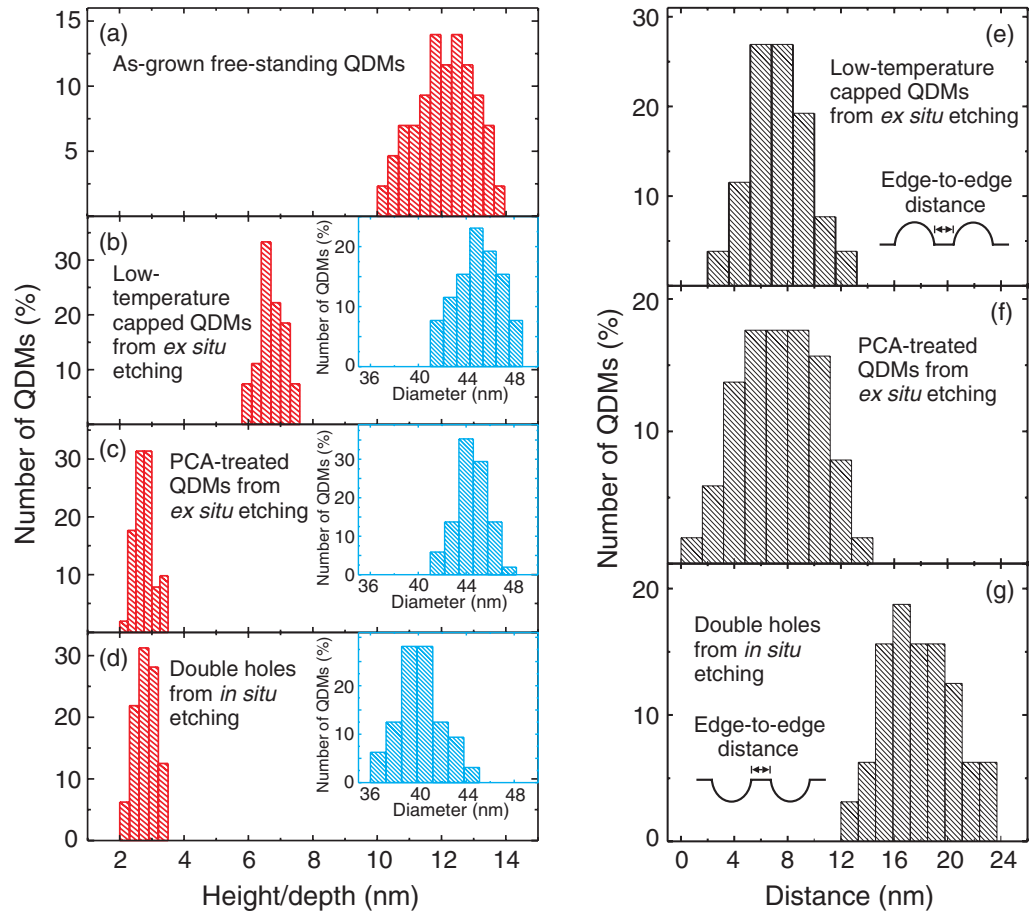
Figure 4. Histograms of QDM height distribution for (a) as-grown free-standing QDMs, (b) QDMs capped at low temperature after *ex situ* etching, (c) QDMs capped by PCA after *ex situ* etching, and (d) depth of double holes produced by AsBr$_3$ *in situ* selective etching of buried QDMs. The insets show corresponding diameter distribution for each sample. (e) and (f) Histograms of edge-to-edge distance for low-temperature capped and PCA treated QDMs, respectively. (g) Histogram of edge-to-edge distance for double holes.

step is applied after the QDMs are capped with 2 nm GaAs, the residual unetched GaAs on top of the initial InAs wetting layer (WL) is about 1.5 nm. The measured hole depth (2.8 nm) is larger than the thickness of the residual GaAs layer, indicating that not only are the buried QDMs removed completely, but also part of the GaAs below the QDMs is removed. The hole depth determined after *in situ* etching, possibly affected also by tip artifacts, cannot be used to gather quantitative information on the QD height.

While the height is strongly affected by the capping, the base diameter of the QDMs does not vary much for different cases. The insets in figures 4(b), (c) and (d) show the corresponding diameter histograms for each sample. Similar diameters are found for PCA and low-temperature capped QDMs, while slightly smaller values are obtained for double holes, which could be due to the details of the *in situ* etching process and AFM tip convolution effects. The comparable diameter for these two *ex situ* etched samples suggests that only the top part of the QDMs is removed during the PCA process, while the diameter of the QDs is not affected. In fact, this
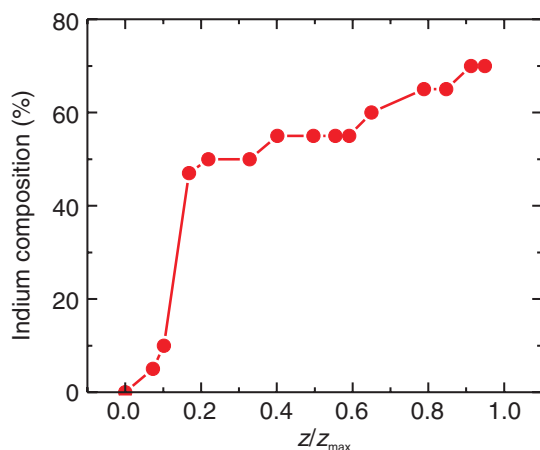
Figure 5. Indium composition of QDMs as a function of normalized height extracted from anomalous x-ray scattering measurements. The maximal height of the QDMs is defined as z_{max}.

effect has been employed to tune the emission of QDs because the transition energy mainly depends on the vertical confinement [24, 32].

The right panel of figure 4 displays the edge-to-edge distance, i.e. the width of GaAs barrier between two QDs composing a QDM, for the three etched samples. Not surprisingly, the interdot distance for PCA and low-temperature capped QDMs shows a similar distribution in figures 4(e) and (f). The observation agrees well with the distribution of the QDM diameter. This phenomenon can be understood in terms of material transport during the capping process. Our result suggests that material migration occurs only at the top of the QDMs and the base diameter of the QDs composing a QDM stays unaffected, as otherwise the highly intermixed InGaAs around the QDMs would be etched away, leading to a larger edge-to-edge distance and a smaller QD diameter. The *in situ* etching provides only a qualitative picture of the distribution of the In-rich region below the thin capping layer; therefore, a larger interdot distance of about 18 nm in figure 4(g) for the double holes is obtained due to its limitation. Moreover, tip convolution effects can also not be ruled out in this case, which is more conspicuous when measuring a small concave surface.

The selective etching combined with surface morphology investigation provides structural information on the size and shape of the buried QDMs, yet no access to In composition. The In composition profile in the QDMs as a function of the distance from the substrate level was previously determined by anomalous x-ray scattering measurements [18] and is reported in figure 5, where z/z_{max} indicates the distance from the substrate (at $z = 0$) normalized to the height of the QDMs (z_{max}). We use these data to extract the In composition inside the PCA-treated QDMs, assuming that only the top part of PCA QDMs is removed and otherwise the In concentration for PCA QDMs and as-grown QDMs is the same.

4. Modeling of the QDM coupling

The selective wet chemical etching, which allows us to access the QDMs encapsulated in a GaAs matrix, provides valuable information on the shape and size of the QDs in our QDMs.
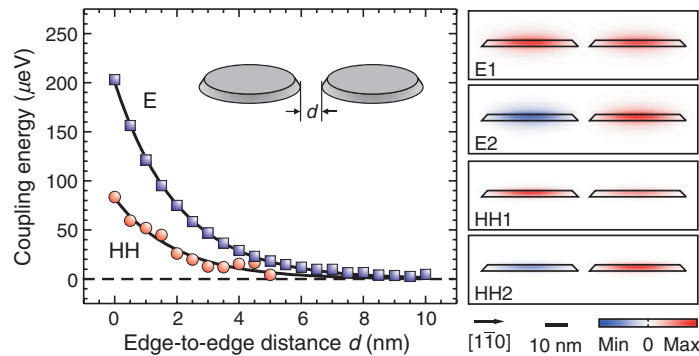
Figure 6. Coupling energy of the ground state electron (E) and heavy hole (HH) as a function of QD edge-to-edge distance in a molecule. The inset shows schematics of the geometry in the model. Symmetric and antisymmetric wavefunctions for the electron (E1 and E2) as well as HH (HH1 and HH2) are illustrated at the right panel for $d = 5$ nm.

Based on the structural parameters obtained from this selective etching and the profile of In concentration derived from the anomalous x-ray scattering data, we are able to calculate the 3D electron (hole) wavefunction and the coupling energy of the lateral QDMs.

In this model, we first perform the calculation of strain states in and around QDs by minimization of the strain energy of the system consisting of two closely spaced QDs and the surrounding GaAs matrix. The finite element method and continuum elasticity are applied throughout this calculation. Once the strain profiles are obtained, the strain-induced band-edge shifts are taken into account for the electron (hole) wavefunction calculation. Deformation potential theory is used to calculate these shifts [33]. For the wavefunction calculation, the Schrödinger equation is solved for the electron and heavy hole (HH) bands using a single-band effective-mass approximation. Material parameters have been extracted from [34] and the finite element method is used in this calculation. The results are the energy eigenvalues of the quantized electronic state and the eigenvector, which is the 3D wavefunction profile of the corresponding state.

The geometry of the QDs in the QDM is taken as follows: the two QDs are assumed to be identical in size, shape and composition profile and the WL is neglected. Each QD has a truncated cone shape with a base diameter of 42 nm and a top diameter of 37 nm. The QD height is taken to be 2.6 nm while the In composition inside each QD increases from 30% at the base to 50% at the top. To investigate the interdot coupling, the edge-to-edge distance d between the two QDs is varied from 0 to 10 nm. All these parameters are consistent with the experimentally observed results presented in the former section within the experimental uncertainty.

The left panel of figure 6 shows the coupling energy (the energy difference between symmetric and antisymmetric states) of both the electron (E) and HH as a function of the edge-to-edge distance d between the QDs in our modeled QDM. As expected, the coupling energies increase when the edge-to-edge distance is decreased. For perfectly identical QDs, when d is significantly large both the electron and HH quantized energies are twofold degenerate and the two QDs show no appreciable coupling. When d decreases, both the electron and HH ground state split into symmetric and antisymmetric states E1 and E2 and HH1 and HH2,

respectively. The amplitude of the coupling energy increases exponentially when d is decreased. As expected, the maximum coupling energy is obtained when the QDs touch each other ($d = 0$ nm).

The coupling energy for the electron is generally higher than that of the HH at the same distance. This is due to the fact that the coupling originates from the effect of carrier tunneling through the interdot barrier. Other coupling mechanisms, such as dipole–dipole coupling between excitons localized in separate QDs, cannot be addressed with the simple model considered here. A thinner barrier, which corresponds to small d, provides larger probability of tunneling. The HH wavefunctions are typically more localized inside the QDs since the HH effective mass is larger than that of the electron. The right panel of figure 6 shows the cross-sectional profile of the QDM wavefunctions along the $[1\bar{1}0]$ direction at $d = 5$ nm. The ground state electron wavefunction (E1) and HH wavefunction (HH1) show a symmetric wavefunction pattern with the maximum near the center of each QD, while the antisymmetric electron (E2) and HH (HH2) wavefunctions are observed as the 'first excited state' for the QDM. In our calculation, the two lowest hole states appear localized in each QD for $d > 5$ nm (not shown here), because of the limited resolution of the mesh used in the finite element calculation. At shorter distance $d \lesssim 5$ nm, the HH wavefunction shows symmetric and antisymmetric wavefunctions similar to those of the electron.

It is noteworthy that the coupling energies obtained from the lateral QDM are generally much smaller than those of vertical QDMs [6] since typically the overlap of the wavefunctions in the vertical geometry is larger than that in the lateral geometry. However, our calculated electron coupling energy is consistent with the value obtained experimentally (200 μeV versus 180 μeV) and the qualitative prediction reported in [19, 21]. This value agrees with the former prediction that the quantum coupling is due to the electron tunneling [19, 21]. Two identical QDs are assumed in this calculation. However, in reality, due to the inherent fluctuations in size, shape and In composition, the two QDs are never identical. Therefore, an electric field will normally be required to compensate for the difference and bring the two QDs into resonance.

5. Micro-PL of single QDMs

The QDM emission is blueshifted by PCA, which results in an emission energy of 1.28–1.39 eV for ensemble QDMs [18]. The transition energy estimated from the calculation for a single QDM is around 1.33 eV, in good agreement with the experimental observation. We measure single QDM PL using a tunable Ti : sapphire laser working in the continuous wave mode. In such micro-PL measurements, the focused laser spot is about 1 μm in diameter. This small spot size together with the low QDM density allows us to examine one single QDM at a time. The PL signal is collected with the same objective, analyzed by a 0.75 m spectrometer and detected by a liquid-nitrogen-cooled charge-coupled device having a resolution of approximately 10 μeV in the spectral range of interest.

Single QDM spectra for two different QDMs obtained at 4 K are presented in figure 7. The different QDMs exhibit common spectral features and similar behavior with excitation power density (P_{Exc}). At low P_{Exc} the spectrum is dominated by two intense PL lines, labeled X1 and X2 (see figures 7(a) and (c)), however, two less intense lines, labeled Y and Z, are also invariably present. The integrated PL intensities of all four emission lines exhibit linear dependence on P_{Exc} [19]. Therefore, we assign the dominant PL lines X1 and X2 to neutral excitonic recombination and the lower energy lines Y and Z to (negatively) charged excitonic
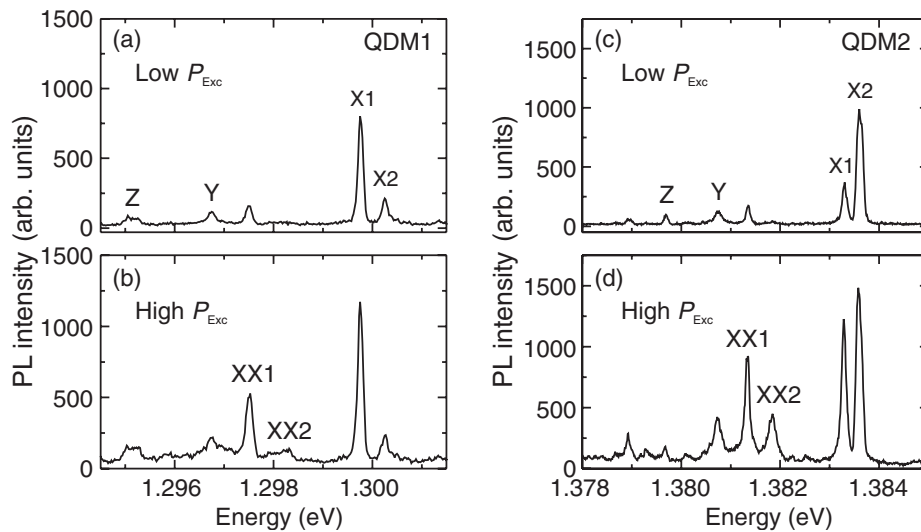
Figure 7. Micro-PL spectra of two typical single QDMs that emit at different energies at different P_{Exc}. The spectra were recorded at 4 K.

recombination for the two QDs in the QDM. With increasing P_{Exc}, two additional lines, XX1 and XX2 (see figures 7(b) and (d)), appear displaying a super-linear P_{Exc}-dependence which indicates that they originate from biexcitonic recombination [19]. The assignment of the PL lines to specific radiative recombination processes in the QDM is supported by the results obtained from photon correlation measurements, which show the intensity-cross-correlations between the different PL lines as well as their temporal behavior [19, 35]. Furthermore, in [19], quantum coupling is reported and its origin is attributed to an interdot electron tunneling mechanism.

6. Laterally ordered QDMs grown on a pre-patterned substrate

For possible future application of the QDM structure in nano-optoelectronic device applications, positioning control of QDMs is required, since the integration of such devices on a single chip is possible only when the nucleation position of QDs on the substrate surface is known in advance. This precise positioning of QDMs can be achieved by growing them on pre-patterned substrates [36]. To realize devices based on single QDMs, dilute arrays of ordered QDMs are necessary.

Here, we demonstrate that it is possible to control the position of QDMs by pre-patterning with a very dilute hole array on the surface, as shown in figure 8. To do this, we have defined small holes, 80 nm wide and 20 nm deep, using conventional electron beam lithography and wet chemical etching [37]. Following *ex situ* cleaning of the surface using solvents, the remaining oxide layer is removed *in situ* by exposure to a hydrogen atom flux. The overgrowth then consists of 7 nm GaAs at 480 °C and 1.4 ML InAs at approximately 500 °C. Preferential migration of GaAs towards As-terminated facets causes the hole shape to change during the buffer growth [38], leading to the formation of two closely spaced holes only 3–4 nm deep [39]. The lateral spacing between these can be controlled by varying the width of the initial patterned holes. These closely spaced, shallow depressions in the surface act as preferential dot nucleation
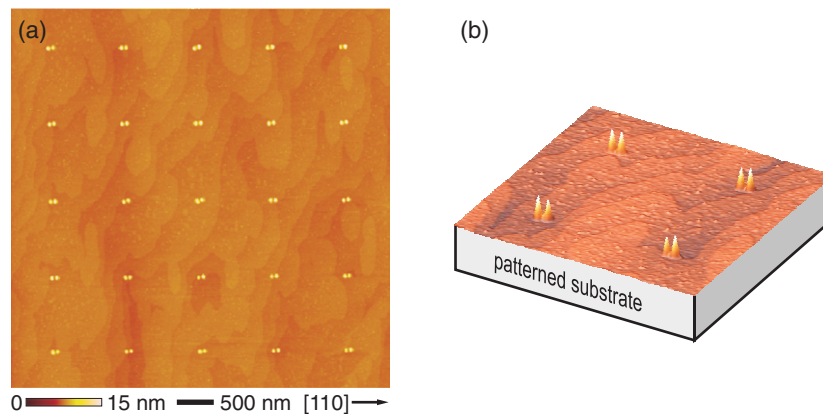
Figure 8. AFM image of (a) ordered QDMs grown on a pre-patterned substrate with a periodicity of 1 μm and (b) 3D perspective view of such ordered QDMs.

sites during the subsequent InAs growth, leading to the ordered array of InAs QDMs aligned in the [110] direction shown here. Figure 8 displays an array of ordered QDMs as well as a 3D perspective view of a 1 μm period QDM array. This wide spacing ensures that each QDM can be addressed individually by micro-PL. Furthermore, another possible advantage of the ordered QDMs lies in the tunability of the interdot distance, achieved by simply varying the width of the initial patterned holes.

7. Triple-terminal devices for deterministic control over QDM coupling

Conventionally, either a vertical *n-i*-Schottky diode or lateral Schottky gates are employed for vertical and lateral QDMs [4]–[7], [19, 20], respectively, to produce the desired electric field for tuning the energy levels of the QDs composing the QDMs. However, in both geometries the contacts have a large dimension and the number of QDMs under the applied electric field is so large that it is not feasible to address only one single QDM at a specific position.

Here, we propose that an additional gate could be placed on top of a single QDM, which should allow not only the coupling between two dots to be tuned, but also the coupling strength. Combining these triple-terminal devices with the growth of QDMs on a pre-patterned substrate, deterministic control of the coupling in only one single QDM at a defined position could be realized.

The fabrication of this triple-terminal device consists of two optical lithography steps and a local oxidation process by AFM, to define the gate at the desired position. To realize such a device, the InAs QDMs are first grown on a pre-patterned substrate followed by 2 nm GaAs capping and 4 min annealing, necessary to tune the QDM emission. A further 58 nm GaAs is deposited to form the upper capping layer. A proper choice of the capping procedure and GaAs thickness is crucial to prevent the mounds with two apexes above the QDM (see also figure 3(b)) from becoming smeared out. However, the cap layer must be thick enough to prevent degradation of the optical properties due to interaction with surface states [40].

The working principle of local oxidation is as follows [41]: first, a 4 nm thick Ge layer is deposited on the GaAs surface. When an AFM tip scans over the surface, a small voltage
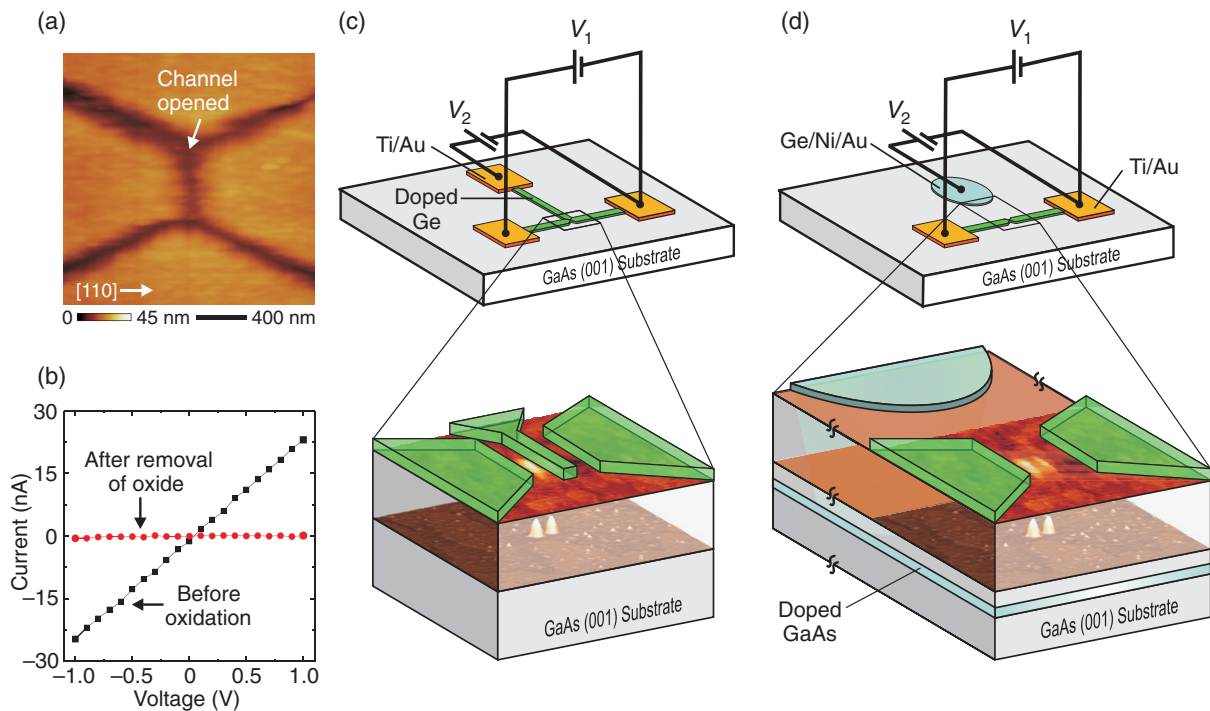
Figure 9. (a) AFM image of the 4 nm thick Ge layer with gaps defined by AFM local oxidation. For the I–V measurement, an external voltage is applied on the left and right sides of the Ge film. (b) I–V curve of the Ge film before and after creating the gaps. (c) and (d) Schematic geometries of the proposed triple-terminal devices defined by optical lithography and AFM local oxidation. AFM local oxidation is performed at the center of the Ge film, and schematics of the zoom-in regions are also shown.

is applied to the tip, which will oxidize locally the thin Ge layer in an environment with a humidity level of approximately 50%. The oxide can be easily removed afterwards by rinsing in water, leaving gaps on the Ge film. As we have shown in figure 9(a), open channels are defined by AFM local oxidation, confirmed by the current–voltage (I–V) measurement in figure 9(b). Before AFM local oxidation, the Ge layer has a resistance of about 50 MΩ, which can easily be deduced from the I–V curve. After removing the oxide, the resistance is above 5 GΩ, which is a clear indication that the oxidation process opens a gap and isolates the Ge film.

To fabricate the triple-terminal device, standard optical lithography will be applied first to create three thick Ti/Au pads with 50–100 μm lateral size, shown in figure 9(c). The three pads will be used afterwards for bonding on to a chip carrier. In the second lithography step, a 4 nm thick T-shaped doped Ge stripe between the three pads will be thermally evaporated. To ensure that the mounds produced by overgrowth of QDMs are still distinguishable by AFM, the Ge layer must be thin enough so that the surface modulation produced by the overgrowth is preserved (clearly visible in figures 9(c) and (d)). The film must also still be transparent to light. Once a QDM below the central region of the T-shaped conducting stripes is located by AFM, we can perform local oxidation around the QDM to open two gaps for the two side gates, leaving only a thin strip exactly between the two dots not oxidized (see the zoom-in of the

T region in figure 9(c)). The advantage of local oxidation is the very precise positioning of the top gate and also the width of the top gate above the QDM is limited only by the resolution of the AFM lithography.

Applying a gate voltage V_1 across the QDM allows the two QDs composing a QDM to be brought into resonance. Moreover, we could also apply a gate voltage V_2 above the QDM so that the potential between the two QDs could also be tuned, namely the strength of coupling, similar to a transistor. In this way, one can scan V_1 and V_2 simultaneously to obtain a 3D map of the coupling behavior. This proposed concept is easy to realize for lateral geometry. However, in the case of vertical configuration, the fabrication of the third gate at the side of the QD stack is quite challenging.

Another possibility to modify the barrier is shown in figure 9(d). In this case, a thin doped layer is grown below the QDMs and conducted by an ohmic contact made of Ni/Ge/Au. Two side gates will be fabricated with a similar method described above (see figure 9(d)). This configuration allows the electron or HH wavefunctions to be pushed up or down by V_2. Because of the non-cylindrical geometry of the QDs, this should result in a change of the effective barrier between the two dots, i.e. how strongly the two QDs are coupled.

In reality, it is desirable to fabricate more than one device on spatially well-defined QDMs on one sample. By defining marker structures with electron beam lithography at the same time as defining the holes for site-controlled QDM formation, we should be able to align the contacts with respect to the QDMs. Knowing the periodicity and size of the pattern, it will then be possible to fabricate arrays of devices, each of which are defined on top of a single QDM. The concepts we proposed could open up new pathways to fully controllable tuning of QDM coupling relative to the conventional gate geometry.

8. Summary and outlook

We have investigated in detail the structure and properties of InGaAs QDMs. Based on an approach combining selective etching and AFM imaging, the 3D morphology of the InGaAs QDMs embedded in a GaAs matrix can be determined. The interdot coupling energy is estimated within a single-band effective-mass approximation, using structural parameters deduced from this uncapping experiment. We have demonstrated site-controlled growth of an ordered array of QDMs and we propose two concepts for a triple-terminal device, which would allow us to access a single QDM at a predefined position and to tune the coupling behavior. Integration of such devices on periodically arranged QDMs could lead to deterministically controlled devices based on QDMs.

Acknowledgments

IOP Institute of Physics ⊕ DEUTSCHE PHYSIKALISCHE GESELLSCHAFT

References

[1] Loss D and DiVincenzo D P 1998 *Phys. Rev.* A **57** 120–6
[2] Burkard G, Loss D and Divincenzo D P 1999 *Phys. Rev.* B **59** 2070–8
[3] Koppens F H L, Buizert C, Tielrooij K J, Vink I T, Nowack K C, Meunier T, Kouwenhoven L P and Vandersypen L M K 2006 *Nature* **442** 766–71
[4] Krenner H J, Sabathil M, Clark E C, Kress A, Schuh D, Bichler M, Abstreiter G and Finley J J 2005 *Phys. Rev. Lett.* **94** 057402
[5] Ortner G, Bayer M, Lyanda-Geller Y, Reinecke T L, Kress A, Reithmaier J P and Forchel A 2005 *Phys. Rev. Lett.* **94** 157401
[6] Stinaff E A, Scheibner M, Bracker A S, Ponomarev I V, Korenev V L, Ware M E, Doty M F, Reinecke T L and Gammon D 2006 *Science* **311** 636–9
[7] Krenner H J, Clark E C, Nakaoka T, Bichler M, Scheurer C, Abstreiter G and Finley J J 2006 *Phys. Rev. Lett.* **97** 076403
[8] Bester G and Zunger A 2005 *Phys. Rev.* B **72** 165334
[9] Schmidt O G, Deneke Ch, Kiravittaya S, Songmuang R, Heidemeyer H, Nakamura Y, Zapf-Gottwick R, Müller C and Jin-Phillipp N Y 2002 *IEEE J. Sel. Top. Quantum Electron.* **8** 1025–34
[10] Bracker A S, Scheibner M, Doty M F, Stinaff E A, Ponomarev I V, Kim J C, Whitman L J, Reinecke T L and Gammon D 2006 *Appl. Phys. Lett.* **89** 233110
[11] Songmuang R, Kiravittaya S and Schmidt O G 2003 *Appl. Phys. Lett.* **82** 2892–4
[12] Lippen T V, Nötzel R, Hamhuis G J and Wolter J H 2004 *Appl. Phys. Lett.* **85** 118–20
[13] Suraprapapich S, Shen Y M, Odnoblyudov V A, Fainman Y, Panyakeow S and Tu C W 2007 *J. Cryst. Growth* **301–302** 735–9
[14] Hanke M, Schmidbauer M, Grigoriev D, Schäfer P, Köhler R, Metzger T H, Wang Zh M, Mazur Yu I and Salamo G J 2006 *Appl. Phys. Lett.* **89** 053116
[15] Yamagiwa M, Mano T, Kuroda T, Tateno T, Sakoda K, Kido G, Koguchi N and Minami F 2006 *Appl. Phys. Lett.* **89** 113115
[16] Lee J H, Wang Zh M, Strom N W, Mazur Yu I and Salamo G J 2006 *Appl. Phys. Lett.* **89** 202101
[17] Kiravittaya S, Songmuang R, Jin-Phillipp N J, Panyakeow S and Schmidt O G 2003 *J. Cryst. Growth* **251** 258–63
[18] Wang L, Rastelli A, Kiravittaya S, Songmuang R, Schmidt O G, Krause B and Metzger T H 2006 *Nanoscale Res. Lett.* **1** 74–8
[19] Beirne G J, Hermannstädter C, Wang L, Rastelli A, Schmidt O G and Michler P 2006 *Phys. Rev. Lett.* **96** 137401
[20] Wang L, Rastelli A, Kiravittaya S, Benyoucef M and Schmidt O G 2006 *Preprint* cond-mat/0612701v3
[21] Beirne G J, Hermannstädter C, Wang L, Rastelli A, Müller E, Schmidt O G and Michler P 2007 *Proc. SPIE* **6471** 647104
[22] Szafran B and Peeters F M 2007 *Phys. Rev.* B **76** 195442
[23] Zhu J and Xu D 2007 *Appl. Phys. Lett.* **90** 261119
[24] Wang L, Rastelli A and Schmidt O G 2006 *J. Appl. Phys.* **100** 064313
[25] Cho S O, Wang Zh M and Salamo G J 2005 *Appl. Phys. Lett.* **86** 113106
[26] Placidi E, Arciprete F, Sessi V, Fanfoni M, Patella F and Balzarotti A 2005 *Appl. Phys. Lett.* **86** 241913
[27] Costantini G, Rastelli A, Manzano C, Acosta-Diaz P, Songmuang R, Katsaros G, Schmidt O G and Kern K 2006 *Phys. Rev. Lett.* **96** 226106
[28] Songmuang R, Kiravittaya S and Schmidt O G 2003 *J. Cryst. Growth* **249** 416–21
[29] Ding F, Wang L, Kiravittaya S, Müller E, Rastelli A and Schmidt O G 2007 *Appl. Phys. Lett.* **90** 173104
[30] Heidemeyer H, Kiravittaya S, Müller C, Jin-Phillipp N Y and Schmidt O G 2002 *Appl. Phys. Lett.* **80** 1544–6
[31] Joyce P B, Krzyzewski T J, Bell G R and Jones T S 2001 *Appl. Phys. Lett.* **79** 3615–7
[32] Garcia J M, Mankad T, Holtz P O, Wellman P J and Petroff P M 1998 *Appl. Phys. Lett.* **72** 3172–4

[33] Van de Walle C G 1989 *Phys. Rev.* B **39** 1871–83

[34] Li E H 2000 *Physica* E **5** 215–73

[35] Hermannstädter C, Beirne G J, Wang L, Rastelli A, Schmidt O G and Michler P 2006 *AIP Conf. Proc.* **893** 875–6

[36] Schmidt O G (ed) 2007 *Lateral Alignment of Epitaxial Quantum Dots* (Berlin: Springer)

[37] Atkinson P, Ward M B, Bremner S P, Anderson D, Farrow T, Jones G A C, Shields A J and Ritchie D A 2006 *Japan. J. Appl. Phys.* **45** 2519–21

[38] Kiravittaya S, Heidemeyer H and Schmidt O G 2004 *Physica* E **23** 253–9

[39] Heidemeyer H, Müller C and Schmidt O G 2004 *J. Cryst. Growth* **261** 444–9

[40] Wang C F, Badolato A, Wilson-Rae I, Petroff P M, Hu E, Urayama J and Imamoglu A 2004 *Appl. Phys. Lett.* **85** 3423–5

[41] Heinzel T, Held R, Lüscher S, Ensslin K, Wegscheider W and Bichler M 2001 *Physica* E **9** 84–93